Magnetization and exciton spectroscopy of the diluted magnetic semiconductor $Cd_{1-x}Cr_xS$

M. Herbich, W. Mac, and A. Twardowski
Institute of Experimental Physics, Warsaw University, Hoża 69, 00-681 Warsaw, Poland

K. Ando
Electrotechnical Laboratory, Tsukuba Science City, Ibaraki 305, Japan

Y. Shapira
Physics Department, Tufts University, Medford, Massachusetts 02155

M. Demianiuk
Institute of Technical Physics, Military Academy of Technology, 00-908 Warsaw, Poland

(Received 5 February 1998)

Free-exciton magnetoreflectance and magnetization are used to study the p-d exchange interaction of $Cd_{1-x}Cr_xS$ ($x=0.0024$, 0.0031, and 0.0033). Magnetization data are well described by a simple crystal-field model taking into account static, tetragonal Jahn-Teller distortion suffered by Cr^{2+} ions, as well as the hexagonal crystal field of CdS. In effect, a strong magnetic anisotropy of a single Cr^{2+} ion was found. From the heavy-hole exciton splitting, and the Cr^{2+} ion spin deduced from magnetization data, the p-d exchange parameter was evaluated as $N_0\beta=+0.48\pm0.05$ eV, using the previously obtained s-d exchange parameter: $N_0\alpha=+0.22\pm0.01$ eV. These exchange parameters provide a reasonable description of the exciton splittings for a magnetic field oriented along or perpendicularly to the crystal hexagonal axis. [S0163-1829(98)02727-1]

I. INTRODUCTION

Diluted magnetic semiconductors (DMS), also known as semimagnetic semiconductors, are based on typical II-VI, III-V, or IV-VI semiconductors for which a controlled fraction of nonmagnetic cations is substituted by magnetic elements.[1] DMS bridge the physics of semiconductors and the physics of magnetic materials, since they retain good semiconductor properties characteristic of their hosts, and at the same time may be regarded as random magnetic systems of localized magnetic moments. The class of DMS is rather broad: a large variety of host lattices and different magnetic ions can be used to produce DMS. All these features made DMS attractive materials for studies during the last two decades. Magneto-optical effects were of particular interest since, due to strong exchange interaction between band carriers and magnetic ions' spins, they are enhanced by orders of magnitude with respect to the nonmagnetic crystals (e.g., Faraday rotation and Zeeman band splitting).[1] The exchange interaction between conduction band (cb) and transition metal (TM) magnetic ions such as Mn^{2+}, Fe^{2+} or Co^{2+} (s-d exchange) results largely from direct (potential) exchange. The contributing s and d one-electron orbitals are centered on the same ion core, so the s-d exchange should be ferromagnetic (FM). This is indeed the case: for all DMS studied so far the exchange parameter $N_0\alpha$ measuring s-d exchange strength was found to be positive and largely magnetic ion and host lattice independent.[1] The situation for the valence band is different. The p-d exchange is dominated by kinetic exchange, determined by the p-d hybridization,[2–7] for which the main contribution arises from virtual jumps of $p(d)$-type electrons to the orbital already occupied by $d(p)$ electrons. The character of this interaction crucially depends on the energy difference between the involved p and d orbitals.[4,6] For II-VI DMS with at least a half-filled d-shell, such as Mn (d^5), Fe (d^6), and Co (d^7) the p-d exchange is antiferromagnetic (AF) (i.e., exchange parameter $N_0\beta<0$), which was well documented experimentally[1] and explained theoretically.[4] On the other hand for less than a half-filled d-shell theory predicts the possibility of a ferromagnetic p-d exchange ($N_0\beta>0$).[3,4,6] Recently ferromagnetic p-d exchange was observed for ZnS, ZnSe, and ZnTe doped with Cr (d^4).[8–11] This observation was of crucial importance for testing theoretical models and understanding the exchange mechanisms in DMS.[4]

The problem with (Zn,Cr)-DMS was the low Cr content, which led to rather low band splittings, so that not all the excitonic transitions could be resolved.[8–11] Eventually the difference $N_0\alpha-N_0\beta$ was evaluated, but not the separate $N_0\alpha$, $N_0\beta$ values. Therefore the conclusion of a ferromagnetic p-d exchange was obtained under the assumption that $N_0\alpha\approx+0.2$ eV. Although this assumption seems to be well justified[1–7] it was not supported by any experimental data for (Zn,Cr) DMS. Only recently $N_0\alpha$ was estimated for $Cd_{1-x}Cr_xS$ ($x=0.0024$) by means of spin-flip Raman spectroscopy (SFRS).[12] Although the Cr content is still low this has opened the possibility of direct determination of a p-d exchange parameter for $Cd_{1-x}Cr_xS$.

In this paper we present magnetoreflectance measurements of excitonic interband transitions in $Cd_{1-x}Cr_xS$ crystals, together with magnetization measurements performed on the same samples. Based on these data we evaluated a $N_0\beta$ parameter, which turned out to be positive, indicating FM p-d exchange.

The paper is organized as follows: in Sec. II the theoretical background necessary to interprete the excitonic transi-

 © 1998 The American Physical Society

tions are presented. Experimental details are given in Sec. III. The magnetization data are presented and discussed in Sec. IV, while Sec. V is devoted to magnetoreflectance data and the determination of the exchange parameter $N_0\beta$. We conclude in Sec. VI.

II. THEORETICAL BACKGROUND

The s,p-d exchange interaction between localized magnetic ions, possessing spin $\mathbf{S}=(S_x,S_y,S_z)$ and delocalized band electrons described by the spin $\mathbf{s}=(s_x,s_y,s_z)$ is usually expressed by isotropic Heisenberg-like Hamiltonian:[2,3]

$$\mathcal{H}_{\rm ex}\propto\hat{\mathbf{S}}\cdot\hat{\mathbf{s}}. \tag{1}$$

This form of exchange was shown to be adequate for Mn, Fe, and Co DMS. For Cr-based DMS the general Hamiltonian is expected to be more complex.[3–5] However the experimental results obtained for (Zn, Cr)-based DMS suggested that the Heisenberg part is still the dominant contribution to the s,p-d Hamiltonian.[11] Therefore also for $Cd_{1-x}Cr_xS$ we will restrict the discussion to the Heisenberg term. The Hamiltonian (1) is typically considered within the mean field approximation (MFA) and the virtual crystal approximation (VCA), which gives[1,13,14]

$$\mathcal{H}_{\rm ex}=-xN_0J\langle\mathbf{S}\rangle\cdot\mathbf{s}, \tag{2}$$

where x is the molar fraction of magnetic ions, N_0 is the number of cations per unit volume, J is the exchange constant (proportional to α or β for conduction or valence band, respectively), $\langle\mathbf{S}\rangle$ is the thermodynamic and configurational average value of the localized spins. (In the discussion which follows we ignore the opposite signs of spin and magnetic moment.) For Mn- and Co-based zinc-blende DMS the ion spin was always oriented along the applied magnetic field, no matter what the direction was. This is not the case for Cr^{2+} ion, neither for the zinc-blende host nor for the wurtzite one, as will be shown below (Sec. IV). Moreover for a hexagonal crystal one has to consider orientation of the ion spin relative to the hexagonal crystal axis. These complications will be discussed below.

The Hamiltonian describing the band structure of the DMS can be obtained as a sum of the Hamiltonian (2), and the well known Hamiltonian of the wurtzite crystals.[15–19] The full Hamiltonian matrix for the conduction band, in the center of the Brillouin zone, which includes direct interaction of the band eleltron with the magnetic field, has in the basis $|S\uparrow\rangle$ or $|S\downarrow\rangle$ the following form (see also Refs. 20–22):

$$\mathcal{H}_{\rm cb}=\begin{pmatrix} E_g+\tau_z+\frac{1}{2}g_e\mu_{\rm B}B & \tau_- \\ \tau_+ & E_g-\tau_z-\frac{1}{2}g_e\mu_{\rm B}B \end{pmatrix}\begin{matrix} S\uparrow \\ S\downarrow \end{matrix}, \tag{3}$$

where the z axis was chosen along crystal hexagonal axis c (this convention will be kept in this paper); E_g is the energy gap and g_e is the electron g factor. The exchange interaction is determined here by the components of the mean spin:

$$\tau_z=\tfrac{1}{2}N_0\alpha x\langle S_z\rangle,$$

$$\tau_\pm=\tfrac{1}{2}N_0\alpha x(\langle S_x\rangle\pm i\langle S_y\rangle),$$

Here $\langle S_z\rangle$ is the mean spin component along the hexagonal axis, $\langle S_x\rangle\pm i\langle S_y\rangle$ are the mean spin components perpendicular to the hexagonal axis and $\alpha=\langle S|J|S\rangle$ is the conduction-band exchange constant. Hamiltonian (3) is given for $\mathbf{B}\|z$. For whichever magnetic field direction the splitting of the conduction band has the form:

$$E_{\rm cb\pm}=E_g\pm\frac{1}{2}\sqrt{\sum_{\lambda=x,y,z}(N_0\alpha x\langle S_\lambda\rangle-g_\lambda)^2},$$

where λ denotes the direction of the magnetic field $\mathbf{B}$. It has to be stressed that the conduction band splitting is proportional to the total spin corrected for the g-factor, which generally may not be parallel to its component along magnetic field.

In the similar manner the valence band matrix, written in in the standard basis function set $X_-\downarrow$, $X_-\uparrow$, $X_+\downarrow$, $X_+\uparrow$, $Z\downarrow$, $Z\uparrow$, where $X_\pm=1/\sqrt{2}(X\pm iY)$, has the form:[15–22]

$$\mathcal{H}_{\rm vb}=\begin{pmatrix} \delta_z+\gamma_{hh}^{\parallel} & \delta_- & 0 & 0 & 0 & 0 \\ \delta_+ & -2\Delta_2-\delta_z & -\sqrt{2}\Delta_3 & 0 & 0 & 0 \\ 0 & -\sqrt{2}\Delta_3 & -\Delta_1-\Delta_2-\delta_z & 0 & 0 & \delta_- \\ 0 & 0 & 0 & -\delta_z-\gamma_{hh}^{\parallel} & \delta_- & 0 \\ 0 & 0 & 0 & \delta_+ & -2\Delta_2+\delta_z & \sqrt{2}\Delta_3 \\ 0 & 0 & \delta_+ & 0 & \sqrt{2}\Delta_3 & -\Delta_1-\Delta_2-\delta_z \end{pmatrix}\begin{matrix} X_+\uparrow \\ X_+\downarrow \\ Z\uparrow \\ X_-\downarrow \\ X_-\uparrow \\ Z\downarrow \end{matrix}, \tag{4}$$

where Δ_1 is the hexagonal crystal-field splitting parameter, Δ_2 and Δ_3 are parameters of the spin-orbit interaction.[16] The main effect of magnetic field is indirect, by producing nonzero mean spin $\langle\mathbf{S}\rangle=(\langle S_x\rangle,\langle S_y\rangle,\langle S_z\rangle)$, which components enter the exchange part of the Hamiltonian

$$\delta_z=\tfrac{1}{2}N_0\beta x\langle S_z\rangle,$$

$$\delta_\pm=\tfrac{1}{2}N_0\beta x(\langle S_x\rangle\pm i\langle S_y\rangle),$$

$\beta=\langle X|J|X\rangle$ is the exchange parameter of the valence band. The standard Zeeman term of the electron direct interaction

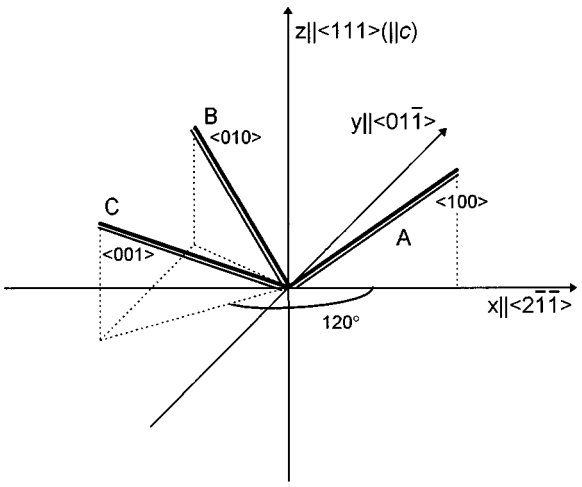

FIG. 1. The Jahn-Teller distortion axes: ⟨100⟩, ⟨010⟩, and ⟨001⟩ in the Cartesian coordinate system, where the ⟨111⟩ is the quantization axis. The momentum operators in the Stevens notation of the crystal-field Hamiltonian are defined for the ⟨100⟩ direction.

has been included only for heavy-hole states for magnetic field along the c axis in the above Hamiltonian (the perpendicular g factor, $g_{hh}^{\perp}$ is zero[23]): $\gamma_{hh}^{\parallel}=\frac{1}{2}g_{\parallel}\mu_B B\cos\vartheta$, where ϑ is the angle between the c axis and the external magnetic field. The direct Zeeman term is, in fact, a correction to the diagonal part only, so it can be added after diagonalization to the hole levels. Unlike conduction-band states particular field orientation now implies the certain mixing between valence-band states, although, as mentioned already, spin may not be colinear with magnetic field.

If the spin is aligned along the hexagonal axis, (i.e., $\langle S_x\rangle=\langle S_y\rangle=0$), then the heavy holes (hh) do not mix with the light holes (lh) or spin-orbit split holes (soh). In effect the hh exchange splitting is proportional to the spin along the c axis, $x\langle S_z\rangle$. On the other hand if the spin is oriented perpendicularly to the hexagonal axis ($\langle S_z\rangle=0$), then for small values of the mean spin, $x(\langle S_x\rangle\pm i\langle S_y\rangle)$ the hh band splitting is negligible. This effect is well known also as the mentioned zero $g_{\perp}$ factor in pure CdS.[23] In general the hh mix with the other bands. This mixing is the reason hh-originated states split, since otherwise operator $\hat{S}_x\pm\hat{S}_y$ has vanishing matrix elements within subspace of pure hh states.

The magnetic anisotropy of Cr-DMS originates from the presence of strong static Jahn-Teller effect of Cr^{2+} ion[11,24,25] along one of three ⟨100⟩, ⟨010⟩, ⟨001⟩ directions (centers A,B,C, respectively—see Fig. 1). For the given, single Cr^{2+} ion its Jahn-Teller distortion axis is an easy axis of the spin orientation. In effect for an arbitrary magnetic field direction there are always nonvanishing both parallel and perpendicular spin components. In the crystal the mean spin results from the averaging over centers A, B, and C. Assuming complete thermal equilibrium[26] the average spin may be expressed in the following way:

$$\langle\mathbf{S}\rangle=\frac{1}{Z}(Z_A\langle\mathbf{S}\rangle_A+Z_B\langle\mathbf{S}\rangle_B+Z_C\langle\mathbf{S}\rangle_C), \tag{5}$$

where Z_n are the partition functions for each of the A,B,C centers in the given magnetic field: $Z_n=\Sigma_i\exp(-E_i^n/k_BT)$, and $Z=Z_A+Z_B+Z_C$. In general for an arbitrary magnetic field direction the spin given by Eq. (5) has nonvanishing components along the c axis ($\langle S_z\rangle$), as well as perpendicular to the c axis ($\langle S_x\rangle+i\langle S_y\rangle$). For certain high symmetry directions of magnetic field ($\mathbf{B}\|\langle 111\rangle$ or $\langle\bar{1}10\rangle$) the perpendicular component vanishes since its contributions from A, B, and C centers sum up to zero.

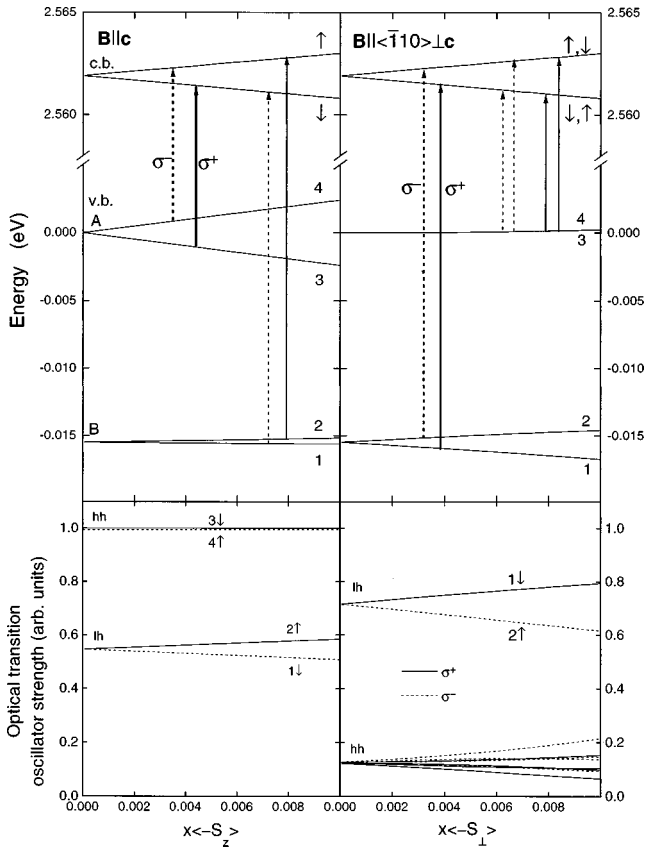

FIG. 2. Calculated band diagram of $Cd_{1-x}Cr_xS$ in $k=0$ as a function of mean spin component (per unit cell): (a) $x\langle S_z\rangle$ for $\mathbf{B}\|c$; (b) $x\langle S_{\perp}\rangle$ for $\mathbf{B}\|\langle\bar{1}10\rangle\perp c$. Arrows indicate optical transitions in circular polarizations (thick arrows represent stronger lines). The bottom picture shows the calculated oscillator strengths of the transitions in σ^- and σ^+ polarizations (the initial and final states are denoted by the hole subband number and conduction spin subband, $\downarrow$ or $\uparrow$).

In Fig. 2 we show the calculated band structure for magnetic field $\mathbf{B}$ parallel ($\mathbf{B}\|\langle 111\rangle$) and perpendicular ($\mathbf{B}\|\langle\bar{1}10\rangle$) to the c axis as a function of the mean spin component along magnetic field, i.e., $x\langle S_z\rangle$ and $x\langle S_{\perp}\rangle=x(\langle S_x\rangle\pm i\langle S_y\rangle)$, respectively (these components correspond to the macroscopic magnetization $M_{\parallel}$ and $M_{\perp}$). The shown $x\langle S_z\rangle$ (or $x\langle S_{\perp}\rangle$) range corresponds to the limit of saturating magnetic fields ($\sim$100 T) for $x=0.005$. Spin components were calculated according to the model presented in Sec. IV. The conduction band splits linearly for both configurations. This results from the fact that exchange splitting of this band, neglecting the direct Zeeman interaction of the band elelctron, is proportional to the total mean spin value, namely, $\langle S\rangle=\sqrt{\langle S_x\rangle^2+\langle S_y\rangle^2+\langle S_z\rangle^2}$, which in our coordinate system reflects the same direction of $\langle S\rangle$ and $\langle S_z\rangle$ for $\mathbf{B}\|c$ or $\langle S\rangle$ and $\langle S_{\perp}\rangle$ for $\mathbf{B}\|\langle\bar{1}10\rangle$.

The situation for the valence band is more complicated.

The heavy-hole subband splits predominantly due to $\langle S_z \rangle$, as was already noted. However, spin operator components perpendicular to the c axis, $\hat{S}_x \pm i\hat{S}_y$, lead to an admixture of the lh and soh states to the hh states (second-order effect). The resulting hh subband A is then sensitive to both $\langle S_z \rangle$ and $\langle S_x \rangle \pm i\langle S_y \rangle$, so strictly speaking the splitting is not linear in the spin component along the given magnetic field. However, in the case of $\mathbf{B} \| c$ (z axis in Fig. 1) the c axis is the triple symmetry axis for all three centers of Jahn-Teller distortions, $\langle 100 \rangle$, $\langle 010 \rangle$, and $\langle 001 \rangle$ (centers A, B, and C, respectively), which are equivalent in this case. In effect, as noted above, perpendicular contributions from $\langle 100 \rangle$, $\langle 010 \rangle$, and $\langle 001 \rangle$ centers cancel together and only spin along the c axis $\langle S_z \rangle$ is nonzero. This way spin $\langle S \rangle = (0,0,\langle S_z \rangle)$ is parallel to the applied magnetic field. The resulting hh splitting is proportional to $\langle S_z \rangle$ and then to the magnetization, as in the case of Mn, Fe, or Co DMS. For lh and soh subbands spin components $\langle S_z \rangle$ contribute linearly to the subband splitting (first-order effect), while the nonlinear band splitting originates from the mixing with other bands (Fig. 2). For the arbitrary magnetic field direction the effects of mixing are expected to be stronger for lh and soh bands than they were for the hh subband, since only the $\hat{S}_x \pm i\hat{S}_y$ operator has nonzero value between the hh and other bands.

For the perpendicular configuration ($\mathbf{B} \perp c$) the hh subband splits, in general, mostly due to the spin component perpendicular to the magnetic field (i.e., $\langle S_z \rangle$ in this case) (Fig. 2). The mixing with the other hole subbands is small, since we consider low x (needless to mention that for higher x mixing would be stronger, making the $\langle S_x \rangle$ component effective). With increasing magnetic field the spin aligns along $\mathbf{B}$ and its perpendicular component $\langle S_z \rangle$ tends to zero, which results in a quenching of the hh band splitting. The contribution of the perpendicular spin component $\langle S_z \rangle$ is the largest for the magnetic field applied along one of the $\langle \bar{2}11 \rangle$ directions. For the particular magnetic field direction along one of the $\langle \bar{1}10 \rangle$ directions the perpendicular mean spin component is zero, since $\langle \bar{1}10 \rangle$ is the symmetry axis for the three Jahn-Teller axes (Sec. IV). Selection rules for hh-to-cb transitions (light polarization refers to the magnetic-field direction) are completely relaxed for low x. The reason is that the heavy-hole states are $(1/\sqrt{2})(X_+ \uparrow \pm X_- \downarrow)$ making all four optical transitions in both σ^- and σ^+ equally probable. On the other hand optical transitions from lh are much more intense than those for hh and selection rules are well pronounced. The purity of transition polarization exceeds 90% even for $\mathbf{B} \| \langle \bar{2}11 \rangle$.

It follows from the above considerations that for magnetic field colinear with the c axis valence band to conduction-band transition energies are simply parametrized by the spin component along the magnetic field, i.e., by the macroscopic magnetization, similarly as for Mn or Fe DMS.[20–22,27] However for the given magnetic field $\mathbf{B}$ not parallel to the c axis or any of the $\langle \bar{1}10 \rangle$ axes the anisotropic magnetic moment appears and the relation between exciton splitting and magnetization is more complicated. This is the consequence of both static, tetragonal Jahn-Teller distortion suffered by Cr^{2+} ions (main contribution) and axial symmetry of CdS crystals (Sec. IV). We note that for cubic Cr-based DMS the hh exchange splitting is proportional to the total Cr^{2+} spin, $\langle \mathbf{S} \rangle$, similar to the conduction-band splitting, but generally is not proportional to the macroscopic magnetization.

III. EXPERIMENT

The $Cd_{1-x}Cr_xS$ crystals were grown from CdS and Cr powders by the modified Bridgman technique, at the Institute of Technical Physics, Military Academy of Technology, Warsaw. Single phase crystals were obtained only for rather low Cr concentrations x, below 0.005. The attempts to grow crystals with higher x resulted in precipitations of Cr_yS_z, similarly to the case of (Zn,Cr)-based DMS. Only single-phase crystals were used for the present study. Since standard methods used to determine crystal composition (atomic absorption or wet chemical analysis) are rather inaccurate for low x values, the chromium content was estimated from the magnetization data, as in (Zn,Cr)-DMS.[11,26] This procedure was based on the assumption that magnetization scales with x, as described in Sec. IV.

Magnetoreflectance spectra of the free excitons were measured in the Faraday configuration (light wave vector parallel to magnetic field) at $T = 2.0$ K and the magnetic field up to $B = 5$ T. The spectra were taken simultaneously in two circular polarizations of light (σ^+ and σ^-). Light polarization always refers to the magnetic-field direction. The magnetic field was oriented either parallel ($\mathbf{B} \| c$) or perpendicular to the hexagonal c axis. Reflectance was measured on freshly cleaved surfaces; neither mechanical polishing nor chemical etching was used. The magnetization of the samples studied optically was measured using a superconducting quantum interference device (SQUID) magnetometer. The temperature, deduced from the pressure over the helium bath, was the same as in the magnetoreflectance measurements. The experimental data were corrected for the diamagnetism of the CdS lattice:[28] $\chi^d_{\mathrm{CdS}} = -3.7 \times 10^{-7}$ emu/g.

IV. MAGNETIZATION

Magnetization (per unit mass) was measured on oriented samples, with magnetic field parallel to the crystal hexagonal axis. Figure 3 shows the results for the samples with $x = 0.0024$, $x = 0.0031$, and $x = 0.0033$ obtained at $T = 2.0$ K. The magnetization varies strongly with magnetic field and no saturation is observed, despite the rather low Cr concentration. This behavior is similar to that observed for (Zn, Cr)-DMS (Ref. 26) and results from the presence of the Jahn-Teller static distortion of the Cr^{2+} ion.[24,25] The shape of magnetization does not depend on the concentration x: the curves displayed in Fig. 3 differ only by a scaling factor. The fact that the shape of the magnetization curve is independent of x means that the interaction between Cr ions is unimportant in our case. This behavior results from the rather low Cr content in our crystals: for $x = 0.003$ about 96% of Cr ions have no nearest magnetic neighbors (NN), so d-d exchange, if any, can be expected for only about 4% of ions. In such a situation the NN interaction strength cannot be deduced from the magnetization data. Therefore, the model that assumes a system of noninteracting Cr ions should provide a reasonable description. In such a model the magnetization per unit mass along the chosen direction denoted by λ is the product of the

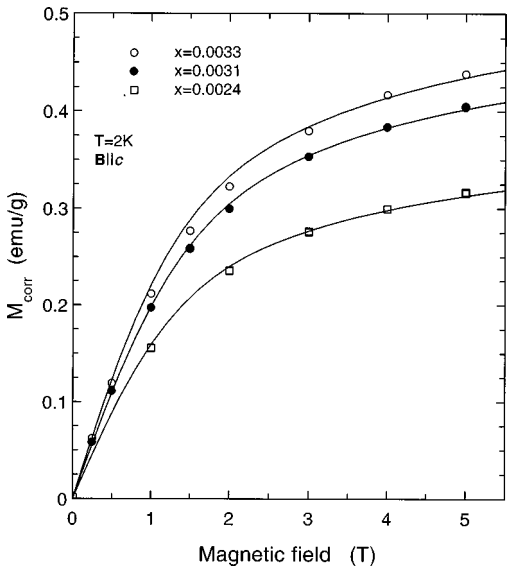

FIG. 3. Magnetization of $Cd_{1-x}Cr_xS$ at $T=2.0$ K for $\mathbf{B}\|c$. Experimental data were corrected for diamagnetic contribution of pure CdS: $\chi^d_{\mathrm{CdS}}=-0.0037$ emu/g (Ref. 28). The solid lines are calculated in the crystal-field model of Cr^{2+} center with one fitting parameter x.

magnetic moment of a single noninteracting ion and the number of the ions in the crystal:

$$M_\lambda^{\mathrm{mass}}=\mu_B\langle M_\lambda\rangle x\,\frac{N_{\mathrm{Av}}}{m_{\mathrm{mole}}}, \tag{6}$$

where $\langle M_\lambda\rangle$ is an average magnetic moment of the ion (averaged over A, B, and C Cr^{2+} centers) along the λ direction, μ_B is Bohr magneton, N_{Av} is Avogadro's number, and m_{mole} is the molar mass of the $Cd_{1-x}Cr_xS$ ''molecule.'' Scaling with x is obvious from Eq. (6). The essential part in describing the magnetization by Eq. (6) is the calculation of the magnetic moment $\langle M_\lambda\rangle$ of a single Cr^{2+} ion. This will be done using crystal field model described below. The average magnetic moment of the Cr^{2+} ion $\langle M_\lambda\rangle$ (in units of μ_B) is the thermodynamical and configurational average of the magnetic moment operator $\hat{M}_\lambda=\hat{L}_\lambda+2\hat{S}_\lambda$:

$$\langle M_\lambda\rangle=\frac{\sum_{i=1}^{N}\langle\varphi_i|\hat{L}_\lambda+2\hat{S}_\lambda|\varphi_i\rangle\exp(-E_i/k_BT)}{\sum_{i=1}^{N}\exp(-E_i/k_BT)}, \tag{7}$$

where k_B is the Boltzmann constant and index i refers to the ith eigenstate of the Cr^{2+} ion (φ_i) with energy E_i.

To obtain eigenstates and energies we generally follow the crystal field model developed by Vallin[24,25] and successfuly used for cubic Cr-DMS.[26,29–32] We recall that the model takes into account tetrahedral crystal field, spin-orbit interaction, static tetragonal Jahn-Teller distortion and magnetic field. In the present case additionally the hexagonal crystal field has to be included. This will be simulated by trigonal distortion, along $\langle 111\rangle$ direction, which will be considered as the c axis. The energy structure of a single Cr^{2+} ion is then described by the Hamiltonian

$$\mathcal{H}=\mathcal{H}_{\mathrm{cf}}+\mathcal{H}_{\mathrm{tr}}+\mathcal{H}_{\mathrm{JT}}+\mathcal{H}_{\mathrm{SO}}+\mathcal{H}_B, \tag{8}$$

where $\mathcal{H}_{\mathrm{cf}}$ is the cubic crystal field of tetrahedral (T_d) symmetry $\mathcal{H}_{\mathrm{tr}}$ is the trigonal crystal field along the c axis, which lowers the symmetry to C_{3v}, $\mathcal{H}_{\mathrm{JT}}$ represents the static Jahn-Teller distortion of tetragonal symmetry, $\mathcal{H}_{\mathrm{SO}}$ is the spin-orbit coupling, and $\mathcal{H}_B$ is Zeeman term representing the effect of magnetic field. In terms of Stevens equivalent operators first three Hamiltonian components are[33]

$$\mathcal{H}_{\mathrm{cf}}=-\frac{2}{3}B_4(\hat{O}_4^0-20\sqrt{2}\hat{O}_4^3), \tag{9a}$$

$$\mathcal{H}_{\mathrm{tr}}=B_2^0\hat{O}_2^0+B_4^0\hat{O}_4^0, \tag{9b}$$

$$\mathcal{H}_{\mathrm{JT}}=\tilde{B}_2^0\hat{\tilde{O}}_2^0+\tilde{B}_4^0\hat{\tilde{O}}_4^0, \tag{9c}$$

where $\hat{O}$ ($\hat{\tilde{O}}$) are operators and B_l^k ($\tilde{B}_l^k$) are constants. Here $\hat{\tilde{O}}$ are operators of the tetragonal distortion along the $\langle 100\rangle$ axis (see Fig. 1) rewritten in the basis for which $\langle 111\rangle$ is the quantization axis (see Appendix). The first term $\mathcal{H}_{\mathrm{cf}}$ splits the free ion ground term (^5D,$L=2$, $S=2$) into an orbital triplet $^5T_2$, which is the ground state and an orbital doublet ^5E. The $^5T_2$-^5E energy separation, $120B_4$ (or $10Dq$), is of the order of 600 meV. Furthermore $^5T_2$ is split by the Jahn-Teller distortion into an orbital singlet $^5B_2$ (ground) and an orbital doublet ^5E located at higher energy by $105\tilde{B}_4^0$ (about 100 meV). The spin-orbit coupling, $\mathcal{H}_{\mathrm{SO}}=\lambda\cdot\hat{\mathbf{L}}\cdot\hat{\mathbf{S}}$, yields further splitting of the spin orbitals: spin quintet $^5B_2$ splits into Γ_1 and Γ_2 (semidoublet ground state), Γ_5 (doublet), and Γ_4 (singlet) (see also Refs. 26, 24, and 25). Due to the fact that the hybridization of the d wave functions with the ligand wave functions is different for the $^5T_2$ and ^5E states, three different parameters λ_{TT}, λ_{TE}, and λ_{EE} are distinguished following the formal definition $\langle\varphi_X|\mathcal{H}_{\mathrm{SO}}|\varphi_Y\rangle=\lambda_{XY}\langle\varphi_X|LS|\varphi_Y\rangle$, where subscripts X or Y denote T or E states.[26,34] The hexagonal crystal field along the c axis lifts the degeneracy of Γ_5 (doublet becomes a semidoublet). Finally external magnetic field, described by the Zeeman term $\mathcal{H}_B=\mu_B(\hat{\mathbf{L}}+2\hat{\mathbf{S}})\mathbf{B}$, lifts all of the remaining degeneracies.

In the present work, we calculated the energy level structure of the Cr^{2+} ion by a numerical diagonalization of the full 25×25 Hamiltonian (8) matrix. Thus all the interactions were fully taken into account, without any approximations. The Hamiltonian matrix contains several parameters. These parameters were chosen to recover the energy structure of the Cr^{2+} ion in CdS in the absence of magnetic field. From the fit to the experimental data of Ref. 25 we obtained $B_4=5.0$ meV (which corresponds to $10Dq=600$ meV), $B_2^0=0.23$ meV, $B_4^0=-0.16$ meV, $\tilde{B}_2^0=-5.8$ meV, and $\tilde{B}_4^0=-1.16$ meV. The spin-orbit coupling parameters are $\lambda_{TT}=1.73$ meV, $\lambda_{TE}=6.0$ meV, and $\lambda_{EE}=6.6$ meV. The energy-level diagram for the five lowest-lying states, calculated for the above parameters and $\mathbf{B}\|c$ is shown in Fig. 4. The mixing between the states for $B\sim3$ T is clearly visible. For higher fields (above 8 T) the mixing becomes less important and the states can be labeled by S_z. We note that the lowest five level manifold can be well described by the effective spin Hamiltonian, with $S=2$.[25] The energies and

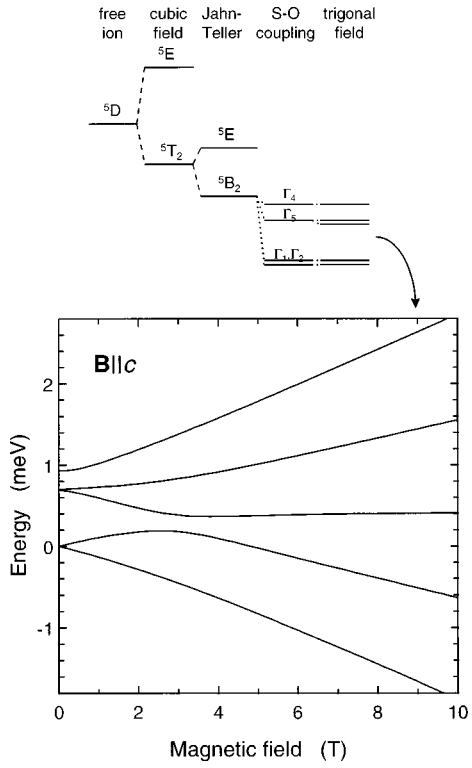

FIG. 4. Energy structure in magnetic field, $\mathbf{B}\|c$, of the five lowest-lying states of Cr^{2+} ion in CdS.

eigenstates obtained from Hamiltonian diagonalization were used for calculating magnetic moment, according to Eq. (7). The result for $\mathbf{B}\|c$ is displayed in Fig. 5, together with the results for the ion spin. First of all we note that the magnetic

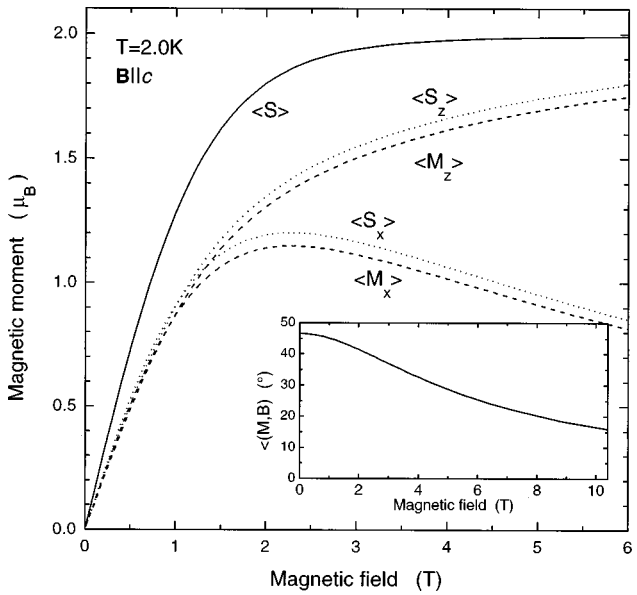

FIG. 5. Calculated spin components of a single Cr^{2+} ion ($\langle 100\rangle$ is the Jahn-Teller distortion axis) as a function of magnetic field ($\mathbf{B}\|c$). $\langle S\rangle$ is the total mean spin, $\langle S_z\rangle$ and $\langle S_x\rangle$ are the spin components along c axis and perpendicular to it, respectively; ($\langle M_z\rangle$ and $\langle M_x\rangle$ are the mean magnetic moment along magnetic field and perpendicular to it, respectively). The inset shows the angle between magnetic field and the total magnetization direction at $T=2.0$ K.

moment is nearly entirely due to the spin. Only a small fraction of $\langle M\rangle$ results from orbital momentum (negative contribution). The most important observation is that magnetic moment is not parallel to the magnetic field, since in addition to the parallel component $\langle M_z\rangle$, there is a substantial perpendicular moment $\langle M_x\rangle$. This effect reflects the importance of JT distortion, which via spin-orbit interaction tries to orient spin along Jahn-Teller $\langle 100\rangle$ axes. The angle between magnetic field and magnetic moment (spin) is close to 45° and decreases with increasing B. Only for very high magnetic fields (tens of T) the alignment effect of magnetic field prevails over JT distortion and the magnetic moment orients along the field. So far we did not discuss the problem of inequivalent Cr^{2+} centers. As discussed previously[24] each Cr^{2+} center suffers one of three JT distortions along $\langle 100\rangle$, $\langle 010\rangle$, and $\langle 001\rangle$. In the absence of magnetic field, all the centers are equivalent. Distortion along $\langle 111\rangle$, which in our case mimics the hexagonal crystal field, does not favor any of the centers. However, arbitrary magnetic field does distinguish between different Cr centers and in general one is dealing with three inequivalent centers. Only for **B** along one of the high symmetry directions does the number of inequivalent centers reduce to two or one. The simplest situation is encountered for $\mathbf{B}\|\langle 111\rangle$, for which **B** is at the angle of 54.7° to each of the JT axes and $\langle 111\rangle$ is the triple symmetry axis for the Jahn-Teller directions. For any other field orientation contributions from different centers have to be considered and averaged with the weights reflecting distribution of the centers. The difficulty is in assigning proper weights to different centers, as was discussed in Refs. 26 and 30. To avoid this complication we verified the model for the case with magnetic field along the hexagonal axis, i.e., for equivalent centers. The calculated magnetization [Eq. (6)] was compared to the experimental data and good agreement was found (Fig. 3). This shows that the crystal-field model well recovers the Cr^{2+} ion energy pattern at our field range. We stress that the Cr concentration, x, was the only adjustable parameter (the resulting x was adopted as Cr concentration).

V. MAGNETOREFLECTANCE

Representative magnetoreflectance spectra in Faraday configuration are demonstrated in Fig. 6 for two cases: $\mathbf{B}\|c$ and $\mathbf{B}\|\langle\bar{1}10\rangle\perp c$. Pronounced exciton A, B, and C structures, corresponding to transitions from hh, lh, and soh valence band to conduction band are observed. The exciton splittings are small even at the highest magnetic fields, which is due to the low chromium content. Nevertheless for $\mathbf{B}\|c$ the splitting of exciton A (hh) is clearly visible. We note that transition at σ^- polarization occurs at lower energy than the σ^+ transition, similarly as for other Cr-based DMS and in contrast with all Mn-, Fe- and Co-based DMS.[1,21,35,36] This observation is compatible with ferromagnetic p-d exchange. The splitting of exciton B is less pronounced, but still visible. On the other hand possible splitting of exciton C is not resolved.

For $\mathbf{B}\perp c$ selection rules for exciton A transitions are relaxed, as noted in Sec. II. The relaxation of the selection rules is complete (all possible transitions are of the same intensity) for $B=0$. For nonzero magnetic fields the intensity of the excitonic transition in polarization σ^- becomes higher

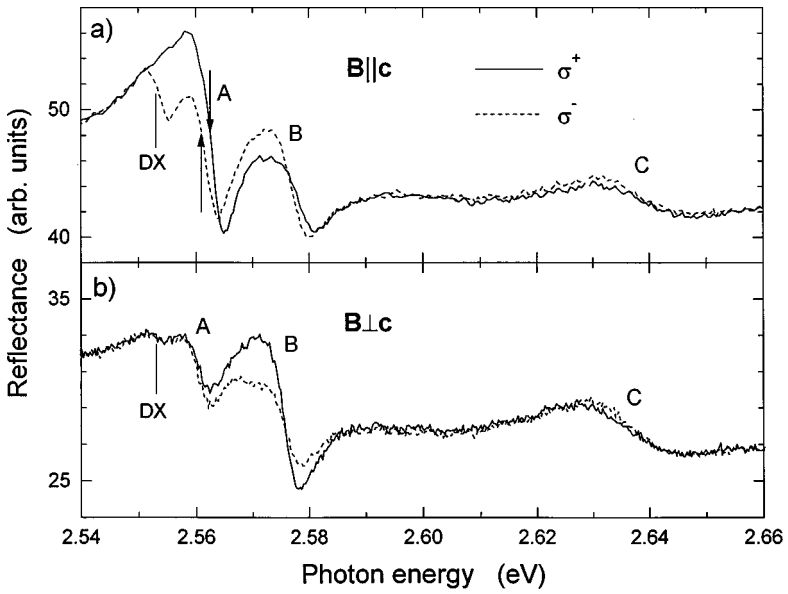

FIG. 6. Representative reflectance spectra of $Cd_{1-x}Cr_xS$ ($x=0.0031$) in Faraday configuration at $T=2.0$ K and $B=5$ T for (a) $\mathbf{B}\|c$, (b) $\mathbf{B}\perp c$. Dashed lines indicate σ^- polarization, solid lines σ^+ polarization. The energies of the heavy-hole excitons are pointed by the arrows.

than in σ^+ but still selection rules are much relaxed. In effect, in both circular polarizations, exciton A has two possible energies, since there are two transition energies (heavy-hole band does not split, Fig. 2). Due to the fact that the energy difference of these two lines is less than or comparable to the linewidth of the exciton spectra, practically the same line is observed for both circular polarizations (Fig. 6). In the case of exciton B the selection rules are much less relaxed but there is practically no splitting of the exciton B. The observed behavior is very different from that encountered for hexagonal Mn, Co, and Fe DMS, for which exciton B practically does not split for $\mathbf{B}\|c$, while for $\mathbf{B}\perp c$ both excitons A and B split pronouncely.[20,21]

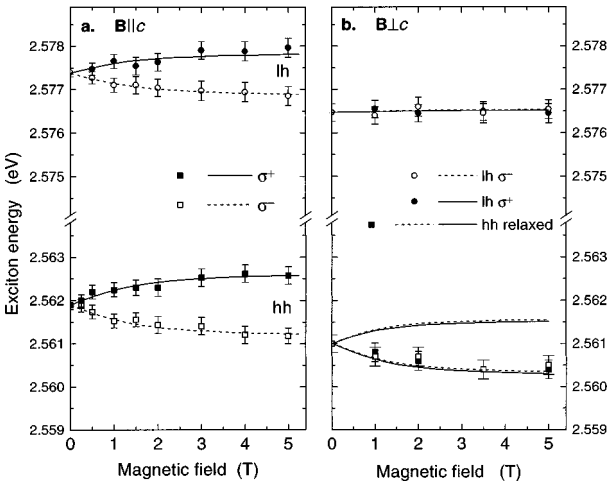

FIG. 7. The light- and the heavy-hole exciton energies of two different $Cd_{1-x}Cr_xS$ samples in Faraday configuration for two orientations of magnetic field: $\mathbf{B}\|c$ (left) and $\mathbf{B}\perp c$ (right). Empty points indicate the σ^- polarization and full points σ^+. The energy position was ascribed to the inflection point of the reflectance structures. The lines indicate calculated energies for the following parameters: $\Delta_1=27.5$ meV, $\Delta=21.7$ meV, $N_0\alpha=+0.22$ eV, $N_0\beta=0.54$ eV (E_g was adjusted to recover zero-field energies). Solid lines represent σ^+, while dashed lines represent σ^- polarizations.

Except for free excitonic structures A, B, and C the bound exciton structure may be observed below exciton A, at energy 2.553 eV (Fig. 6). For $\mathbf{B}\|c$ the bound exciton is visible only for σ^- polarized transitions. This is due to the fact that the donor ground state built of the conduction-band wave function is occupied and then cannot serve as a final state for optical transition. In the case of $\mathbf{B}\perp c$ the initial heavy-hole states for the transitions are well mixed so the transition to the the upper donor state is visible for both polarizations, but is less pronounced due to the hole mixing (Fig. 6).

The sample magnetic field dependence of excitons A and B energy for parallel and perpendicular configurations is shown in Fig. 7. The inflection points of reflectance structures were used to determine exciton energy. In Fig. 8 we present the hh exciton splitting for $\mathbf{B}\|c$, corrected for the Zeeman splitting of pure CdS (0.06 meV/T, as measured by us). This mimics exchange-induced hh exciton splitting. Usually this splitting is used for determination of s,p-d exchange constants.[1,35,14] It follows from Eqs. (3) and (4) and

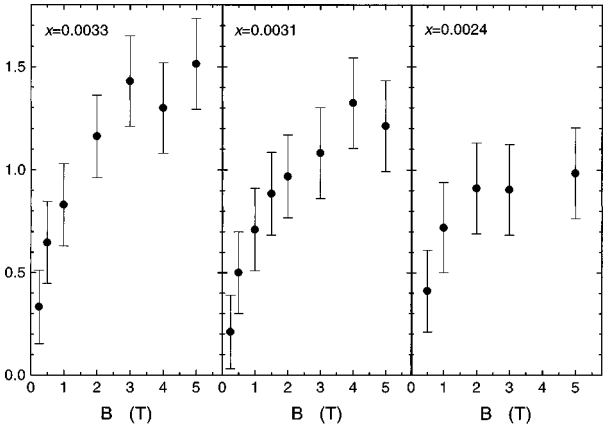

FIG. 8. Heavy-hole exciton splitting of $Cd_{1-x}Cr_xS$ for $\mathbf{B}\|c$ at $T=2.0$ K as a function of magnetic field. Data were corrected for the Zeeman splitting of pure CdS (0.06 meV/T, as measured by us).

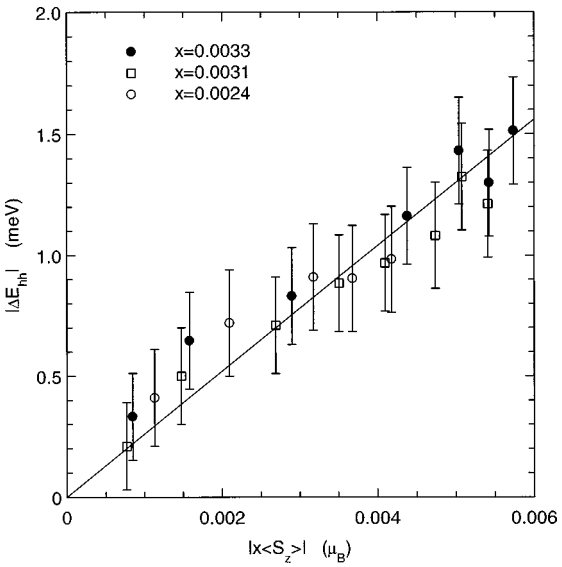

FIG. 9. Heavy-hole exciton splitting of $Cd_{1-x}Cr_xS$ for $\mathbf{B}\|c$ (normalized to the molar fraction of chromium) vs mean spin component of single Cr^{2+} ion, $\langle S_z\rangle$, obtained from the magnetization data. Straight line corresponds to $N_0\alpha - N_0\beta = +0.26$ eV.

the considered equivalence of the Jahn-Teller centers (Sec. II) for $\mathbf{B}\|c$ that the hh exciton exchange splitting is proportional to the spin component along the c axis:

$$\Delta E = (N_0\alpha - N_0\beta)x\langle S_z\rangle + (g_e - g_{\mathrm{hh}}^{\parallel})\mu_{\mathrm{B}}B, \qquad (10)$$

where $x\langle S_z\rangle$ is proportional to the macroscopic magnetization: $x\langle S_z\rangle = k\, x\langle M\rangle$ ($k \approx 0.523$ practically magnetic field independent for our field range[26]). We note that Zeeman splitting of pure CdS is an additive correction to the total splitting ΔE [Eq. (10)], which justifies evaluation of the exchange splitting $\Delta E_{\mathrm{exch}} = (N_0\alpha - N_0\beta)x\langle S_z\rangle$ as a difference between $Cd_{1-x}Cr_xS$ and CdS splittings. Plotting ΔE_{exch} versus magnetization one can directly evaluate exchange parameter $N_0\alpha - N_0\beta$. This method was used for Mn, Co, Fe, and cubic Cr DMS.[8,11,21,13,27,35,14] The plot of ΔE_{exch} versus $x\langle S_z\rangle$ (the latter calculated from the macroscopic magnetization) is displayed in Fig. 9. The stright line corresponds to $N_0\alpha - N_0\beta = +0.26$ eV. Since the conduction-band parameter was evaluated in independent spin-flip Raman scattering experiment as $N_0\alpha = +0.22$ eV, we finally obtained $N_0\beta = +0.48 \pm 0.05$ eV. We note that in the case of nonvanishing perpendicular spin component one should plot $\Delta E_{\mathrm{exch}}/x$ versus $\langle S_z\rangle$ to obtain $N_0\alpha - N_0\beta$.

The evaluated p-d exchange parameter, together with the others, was used for calculating all the excitonic transitions for both magnetic-field configurations. Hamiltonians (3) and (4) are parametrized by the following parameters: E_g, Δ_1, $\Delta = \Delta_2 = \Delta_3$ (so-called quasi-cubic approximation), S_x, S_z, x, $N_0\alpha$, and $N_0\beta$. Since our crystals are rather diluted we used for the first four parameters pure CdS values: $E_g = 2.562$ eV (this parameter does not enter into hh exciton splitting anyway), $\Delta_1 = 27.5$ meV, $\Delta = 21.7$ meV (compare the values in Ref. 19). The result is displayed in Fig. 6 (for E_g, which is slightly x dependent, we adopted the zero field energy of exciton A for a given crystal). Generally speaking the model calculations recover experimental exciton energy field dependence quite well. This is particularly true for hh exciton (A) in parallel configuration. The model predicts strong polarization of both exciton components, in agreement with experimental observation. For perpendicular configuration ($\mathbf{B}\|\langle\bar{1}10\rangle$) our model well reproduces very weak splittings of exciton B. Also strong relaxation of selection rules for hh exciton transitions are predicted. We point out that the difference between exciton splitting in $Cd_{1-x}Cr_xS$ and hexagonal Mn, Co, Fe DMS (for which a very similar overall exciton behavior was observed[20–22]) results mainly from different sign of $N_0\beta$ value for these systems.

In the case of the magnetic field applied along none of the three $\langle 111\rangle$ axes (c axis in hexagonal crystals) nor along one of twelve $\langle 110\rangle$ (one of four $\langle\bar{1}10\rangle$ in hexagonal crystals) the Cr DMS are magnetically anisotropic, as already noted. To some extent a similar situation may be encountered for Fe-DMS, where magnetization is anisotropic, however, for cubic crystals and not very high magnetic fields the anisotropy is rather weak.[37] Thus for Fe DMS Eq. (10) can still be used. For cubic Cr DMS both conduction and hh bands split proportionally to the Cr spin length. Therefore Eq. (10) should be replaced by

$$\Delta E = \{[g_e\mu_{\mathrm{B}}B\,\sin\,\vartheta - (N_0\alpha - N_0\beta)x(\langle S_x\rangle \pm i\langle S_y\rangle)]^2 + [(g_e\cos\,\vartheta - g_{\mathrm{hh}}^{\parallel})\mu_{\mathrm{B}}B - (N_0\alpha - N_0\beta)x\langle S_z\rangle]^2\}^{1/2}. \qquad (11)$$

The only complication is that the spin $\langle\mathbf{S}\rangle$ has to be evaluated from macroscopic magnetization, using the crystal-field model described in Sec. IV. Since $\langle S\rangle$ is not proportional to the magnetization (as $\langle S_z\rangle$ is) hh exciton splitting is no longer parametrized by magnetization directly, as it was for Mn and Co DMS. Still ΔE scales with $\langle S\rangle$, which is Cr concentration and exchange constants $N_0\alpha$, $N_0\beta$ independent. This way the difference $N_0\alpha - N_0\beta$ can be determined directly by comparing ΔE with evaluated mean spin as a function of T and B, $\langle\mathbf{S}(T,B)\rangle$.

Finally we would like to comment on the estimated $N_0\beta$ value. This value is the lowest from all obtained so far for $Zn_{1-x}Cr_xS$, $Zn_{1-x}Cr_xSe$, and $Zn_{1-x}Cr_xTe$.[11] Although no proper calculations of the $N_0\beta$ value were done for Cr-DMS with different host lattices, a naive model of Ref. 11 can be used as a first-order approximation. In this model ferromagnetic p-d exchange results from an empty spin-up d orbital located above the top of the valence band. The magnitude of the interaction ($N_0\beta$) depends on the probability of p-d hopping and energy denominator, i.e., energy difference between the top of the valence band and the d orbital. Following this argument one may expect an increasing $N_0\beta$ value with the top of the valence band approaching the spin-up d level. Such behavior was indeed observed for the series of ZnCrS, $Zn_{1-x}Cr_xSe$, and $Zn_{1-x}Cr_xTe$, for which the valence-band offset (relative d level) is the largest for ZnS and the smallest for ZnTe. Accordingly $N_0\beta$ was the smallest for $Zn_{1-x}Cr_xS$ and the largest for $Zn_{1-x}Cr_xTe$.[11] The valence-band offset for CdS is slightly larger than that of ZnS, so one could expect similar $N_0\beta$ for both sulfides, which is the case. We would like to stress, however, that one should be aware of extending this simple, one-electron reasoning too far, since in some cases it may lead to false conclusions.

VI. CONCLUSIONS

The influence of magnetic field on free exciton at $Cd_{1-x}Cr_xS$ was studied for the field oriented along and perpendicularly to the crystal hexagonal axis. The observed heavy- and light-hole excitons split in a different way than they did for DMS hexagonal crystals with Mn, Fe, or Co. This difference results from the sign (ferromagnetic) and the magnitude of p-d exchange interaction. The value of p-d exchange parameter was estimated from the heavy-hole exciton splitting compared to the Cr^{2+} ion spin calculated within simple crystal field model taking into account static, tetragonal Jahn-Teller distortion experienced by Cr^{2+} ions and hexagonal crystal field of CdS. The validity of these calculations is justified by a very good description of magnetization data by the same model. The role of the spin anisotropy resulting from both hexagonal and tetragonal distortions was pointed out. In this particular case $\mathbf{B}\|c$ heavy-hole exciton splitting is parametrized by the macroscopic magnetization, as it was for Mn- and Co-based DMS, in the spirit of the mean-field and virtual crystal approximations. The determined p-d exchange strength is the smallest among Cr-based DMS, which seems to comply with valence-band offset of CdS, relatively (Zn,Cr)-based DMS.

ACKNOWLEDGMENTS

We acknowledge financial support from The State Committee of Scientific Research (Poland), in particular under Grant No. 2P03B 003 11. Travel funds for A. Twardowski were provided by NATO Grant No. 970440.

APPENDIX A

Here we calculate the momentum operators entering the Jahn-Teller part of the Hamiltonian (8) for the center of the type A (along $\langle 100\rangle$). We recall the expression for the Jahn-Teller distortion Hamiltonian [Eq. (9c)],

$$\mathcal{H}_{\mathrm{JT}}=\tilde{B}_2^0\hat{\tilde{O}}_2^0+\tilde{B}_4^0\hat{\tilde{O}}_4^0,$$

would have the same form as $\mathcal{H}_{\mathrm{tr}}$ [Eq. (9b)] if the chosen quatization axis is one of the three $\langle 100\rangle$ directions. Actually the quantization axis is chosen along the $\langle 111\rangle$ direction since it simplifies calculations (especially for $\mathbf{B}\|c$). Therefore it is necessary to express the $\hat{O}_2^0$ and $\hat{O}_4^0$ operators of the Jahn-Teller Hamiltonian for the turned coordination axes, for which the $\langle 111\rangle$ axis will be the chosen one. These new operators are called $\hat{\tilde{O}}_2^0$ and $\hat{\tilde{O}}_4^0$.

We recall after Ref. 33 that the Stevens equivalent operators appearing in Eqs. (9a) and (9b) are of the following form:

$$\hat{O}_2^0=\hat{J}_z{}^2-J(J+1), \tag{A1}$$

$$\hat{O}_4^0=35\hat{J}_z{}^4-30J(J+1)\hat{J}_z{}^2+25\hat{J}_z{}^2-6(J+1)J+3J^2(J+1)^2, \tag{A2}$$

$$\hat{O}_4^3=\tfrac{1}{4}[\hat{J}_z(\hat{J}_+{}^3+\hat{J}_-{}^3)+(\hat{J}_+{}^3+\hat{J}_-{}^3)\hat{J}_z], \tag{A3}$$

where $\hat{J}_z$, $\hat{J}_-$, and $\hat{J}_+$ are the orbital momentum operators and $J=2$ (in the case of Cr^{2+} ion). First two of the above Stevens operators appear in $\mathcal{H}_{\mathrm{JT}}$, when the Jahn-Teller distortion along $\langle 100\rangle$ states the quantization axis. We refer to this axis as $\tilde{z}$ in the $(\tilde{x},\tilde{y},\tilde{z})$ Cartesian coordinates. Additionally the $\tilde{z}$ axis is chosen in the plane of (x,z) axes of the desired coordinates ($z\|\langle 111\rangle$). In effect the versors of $(\tilde{x},\tilde{y},\tilde{z})$ coordinates are expressed by the (x,y,z) versors in the following way:

$$\begin{aligned}\tilde{e}_x&=\frac{1}{\sqrt{3}}e_z-\frac{1}{\sqrt{3}}e_x+\frac{1}{\sqrt{3}}e_y,\\ \tilde{e}_y&=\frac{1}{\sqrt{3}}e_z-\frac{1}{\sqrt{3}}e_x-\frac{1}{\sqrt{3}}e_y,\\ \tilde{e}_z&=\frac{1}{\sqrt{3}}e_z+\sqrt{\frac{2}{3}}\,e_x.\end{aligned} \tag{A4}$$

Accordingly the ''turned'' momentum operators $(\hat{\tilde{J}}_z,\hat{\tilde{J}}_-,\hat{\tilde{J}}_+)$ take the form

$$\hat{\tilde{J}}_+=(\hat{\tilde{J}}_x+i\hat{\tilde{J}}_y)=\frac{1}{\sqrt{3}}[(1+i)\hat{J}_z-(1+i)\hat{J}_x+(1-i)\hat{J}_y], \tag{A5}$$

$$\hat{\tilde{J}}_-=(\hat{\tilde{J}}_x-i\hat{\tilde{J}}_y)=\frac{1}{\sqrt{3}}[(1-i)\hat{J}_z-(1-i)\hat{J}_x+(1+i)\hat{J}_y], \tag{A6}$$

$$\hat{\tilde{J}}_z=\frac{1}{\sqrt{3}}(\hat{J}_z+\sqrt{2}\hat{J}_x). \tag{A7}$$

The resulting $\hat{\tilde{J}}_z{}^2$ and $\hat{\tilde{J}}_z{}^4$ operators appearing in $\hat{\tilde{O}}_2^0$ and $\hat{\tilde{O}}_4^0$ of $\mathcal{H}_{\mathrm{JT}}$ are

$$\hat{\tilde{J}}_z{}^2=\frac{1}{3}\hat{J}_z{}^2+\frac{2}{3}\hat{J}_x{}^2+\frac{\sqrt{2}}{3}(\hat{J}_z\hat{J}_x+\hat{J}_x\hat{J}_z), \tag{A8}$$

$$\begin{aligned}\hat{\tilde{J}}_z{}^4=&\frac{1}{9}\hat{J}_z{}^4+\frac{4}{9}\hat{J}_x{}^4+\frac{2}{9}[\hat{J}_z\hat{J}_x\hat{J}_z\hat{J}_x+\hat{J}_x\hat{J}_z\hat{J}_x\hat{J}_z+\hat{J}_z\hat{J}_x{}^2\hat{J}_z\\ &+\hat{J}_x\hat{J}_z{}^2\hat{J}_x+\hat{J}_z{}^2\hat{J}_x{}^2+\hat{J}_x{}^2\hat{J}_z{}^2]+\frac{\sqrt{2}}{9}[\hat{J}_z{}^2(\hat{J}_z\hat{J}_x+\hat{J}_x\hat{J}_z)\\ &+(\hat{J}_z\hat{J}_x+\hat{J}_x\hat{J}_z)\hat{J}_z{}^2]+\frac{2\sqrt{2}}{9}[\hat{J}_x{}^2(\hat{J}_z\hat{J}_x+\hat{J}_x\hat{J}_z)\\ &+(\hat{J}_z\hat{J}_x+\hat{J}_x\hat{J}_z)\hat{J}_x{}^2].\end{aligned} \tag{A9}$$

Finally the ''turned'' Stevens operators have the form

$$\hat{\tilde{O}}_2^0=3\hat{\tilde{J}}_z{}^2-J(J+1), \tag{A10}$$

$$\hat{\tilde{O}}_4^0=35\hat{\tilde{J}}_z{}^4-30J(J+1)\hat{\tilde{J}}_z{}^2+25\hat{\tilde{J}}_z{}^2-6(J+1)J+3J^2(J+1)^2. \tag{A11}$$

We stress that these above formulas were calculated only for the center A (Fig. 1). However, we take advantage of the fact that for all three centers A, B, and C, c axis is the triple symmetry axis. Therefore instead of calculating the expressions for the momentum operators for B and C types of centers the equivalent way is to turn the magnetic field direction $\mathbf{B}/|\mathbf{B}|$ (relatively to A direction) to simulate the contribution of the B and C centers.

[1] *Diluted Magnetic Semiconductors*, edited by J. K. Furdyna and J. Kossut, Series on Semiconductors and Semimetals Vol. 25 (Academic Press, New York, 1988); *Diluted Magnetic Semiconductors*, edited by M. Balkanski and M. Averous (Plenum Press, New York, 1991); J. Kossut and W. Dobrowolski, in *Handbook of Magnetic Materials*, edited by K. H. J. Buschow (North-Holland, Amsterdam, 1993), Vol. 7, p. 231.

[2] K. C. Hass, in *Diluted Magnetic Semiconductors*, edited by M. Averous and M. Balkanski (Plenum, New York, 1991); B. E. Larson, K. C. Hass, H. Ehrenreich, and A. E. Carlsson, Solid State Commun. **56**, 347 (1985); B. E. Larson, K. C. Hass, H. Ehrenreich, and A. E. Carlsson, Phys. Rev. B **37**, 4137 (1988).

[3] J. Blinowski, P. Kacman, and H. Przybylińska, Solid State Commun. **79**, 1021 (1991).

[4] J. Blinowski and P. Kacman, Phys. Rev. B **46**, 12 298 (1992); J. Blinowski, P. Kacman, and J. A. Majewski, Acta Phys. Pol. A **88**, 683 (1995); J. Cryst. Growth **159**, 973 (1996).

[5] A. K. Bhattacharjee, G. Fishman, and B. Coqblin, Physica B **117&118B**, 449 (1983).

[6] A. K. Bhattacharjee, Phys. Rev. B **46**, 5266 (1992); **49**, 13 987 (1994).

[7] J. Mašek, Solid State Commun. **78**, 351 (1991).

[8] W. Mac, N. T. Khoi, A. Twardowski, and J. A. Gaj, M. Demianiuk, Phys. Rev. Lett. **71**, 2327 (1993).

[9] W. Mac, Nguyen The Khoi, A. Twardowski, and M. Demianiuk, J. Cryst. Growth **159**, 993 (1996).

[10] W. Mac, Nguyen The Khoi, and A. Twardowski, in *Proceedings of the 22nd International Conference on the Physics of Semiconductors, Vancouver, 1994*, edited by D. J. Lockwood (World Scientific, Singapore, 1995), p. 2569.

[11] W. Mac, A. Twardowski, and M. Demianiuk, Phys. Rev. B **54**, 5528 (1996).

[12] A. Twardowski, D. Heiman, M. T. Liu, and Y. Shapira, and M. Demianiuk, Phys. Rev. B **53**, 10 728 (1996).

[13] J. A. Gaj, J. Ginter, and R. R. Gałązka, Phys. Status Solidi B **89**, 655 (1978).

[14] J. A. Gaj, R. Planel, and G. Fishman, Solid State Commun. **29**, 435 (1979).

[15] J. J. Hopfield, J. Phys. Chem. Solids **15**, 97 (1960).

[16] G. E. Pikus, Zh. Éksp. Teor. Fiz. **41**, 1507 (1961) [Sov. Phys. JETP **14**, 1075 (1962)]; G. L. Bir and G. E. Pikus, *Symmetry and Strain-Induced Effects in Semiconductors* (Wiley, New York, 1974).

[17] S. L. Adler, Phys. Rev. B **126**, 118 (1962).

[18] A. V. Komarov, S. M. Ryabchenko, Yu. G. Semyonov, B. D. Shanina, and N. I. Vitrihovskii, Zh. Éksp. Teor. Fiz. **79**, 1554 (1980) [Sov. Phys. JETP **52**, 783 (1980)].

[19] S. I. Gubarev, Zh. Éksp. Teor. Fiz. **80**, 1174 (1981) [Sov. Phys. JETP **53**, 601 (1981)].

[20] R. L. Aggarwal, S. N. Jasperson, J. Stankiewicz, and Y. Shapira, S. Foner, B. Khazai, and A. Wold, Phys. Rev. B **28**, 6907 (1983).

[21] A. Twardowski, K. Pakuła, I. Perez, P. Wise, and J. E. Crow, Phys. Rev. B **42**, 7567 (1990).

[22] W. Y. Yu, A. Twardowski, L. P. Fu, A. Petrou, and B. T. Jonker, Phys. Rev. B **51**, 9722 (1995).

[23] D. G. Thomas and J. J. Hopfield, Phys. Rev. **175**, 1021 (1968).

[24] J. T. Vallin, G. A. Slack, S. Roberts, and A. E. Hughes, Phys. Rev. B **2**, 4313 (1970).

[25] J. T. Vallin and G. D. Watkins, Phys. Rev. B **9**, 2051 (1974).

[26] W. Mac, A. Twardowski, P. J. T. Eggenkamp, H. J. M. Swagten, Y. Shapira, and M. Demianiuk, Phys. Rev. B **50**, 14 144 (1994).

[27] A. Twardowski, P. Głód, P. Wise, J. E. Crow, and M. Demianiuk, Phys. Rev. B **46**, 7537 (1992).

[28] M. E. Lines and J. V. Waszczak, J. Appl. Phys. **48**, 1395 (1977).

[29] A. Twardowski, T. Fries, Y. Shapira, P. Eggenkamp, H. J. M. Swagten, and M. Demianiuk, J. Appl. Phys. **73**, 5745 (1993).

[30] G. H. McCabe, Y. Shapira, V. Bindilatti, N. F. Oliveira, A. Twardowski, W. Mac, E. J. McNiff, and M. Demianiuk, Solid State Commun. **95**, 841 (1995).

[31] R. Krevet, A. Twardowski, M. von Ortenberg, W. Mac, and M. Demianiuk, Solid State Commun. **87**, 709 (1993).

[32] W. Mac, A. Twardowski, M. E. J. Boonman, A. Wittlin, R. Krevet, M. von Ortenberg, and M. Demianiuk, Physica B **211**, 384 (1995).

[33] A. Abragam and B. Bleaney, *Electron Paramagnetic Ressonance of Transition Metal Ions* (Clarendon Press, Oxford, 1970).

[34] M. E. J. Boonman, W. Mac, A. Wittlin, A. Twardowski, and M. Demianiuk, Acta Phys. Pol. A **88**, 829 (1995).

[35] See, e.g., A. Twardowski, P. Głód, W. J. M. de Jonge, and M. Demianiuk, Solid State Commun. **64**, 63 (1987); D. Scalbert, M. Guillot, A. Mauger, J. A. Gaj, J. Cernogora, C. Benoit a la Guillaume, and A. Mycielski, Solid State Commun. **76**, 977 (1990); O. W. Shih, R. L. Aggarwal, Y. Shapira, S. H. Bloom, V. Bindillati, R. Kershaw, K. Dwight, and A. Wold, Solid State Commun. **74**, 455 (1990); W. Mac, M. Herbich, Nguyen The Khoi, A. Twardowski, Y. Shapira, and M. Demianiuk, Phys. Rev. B **53**, 9532 (1996).

[36] See, e.g., D. U. Bartholomew, E. H. Suh, A. K. Ramdas, S. Rodriguez, U. Debska, and J. K. Furdyna, Phys. Rev. B **39**, 5865 (1989); X. Liu, A. Petrou, B. T. Jonker, J. J. Krebs, G. A. Prinz, and J. Warnock, J. Appl. Phys. **55**, 1023 (1989); M. Nawrocki, F. Hamdani, J. P. Lascaray, Z. Golacki, and J. Deportes, Solid State Commun. **77**, 111 (1991); M. Inoue, N. Adachi, I. Mogi, G. Kido, and Y. Nakagawa, Physica B **184**, 441 (1993);

[37] T. Fries, Y. Shapira, A. Twardowski, E. J. McNiff, T. Q. Vu, R. Kershaw, K. Dwight, and A. Wold, Phys. Rev. B **49**, 11 870 (1994).